



Pronounced northward shift of the westerlies during MIS 17 leading to the strong 100-kyr ice age cycles

María Fernanda Sánchez Goñi^{a,b,*}, Patrizia Ferretti^c, Josué M. Polanco-Martínez^{b,d}, Teresa Rodrigues^{e,f}, Montserrat Alonso-García^{e,f}, Francisco Javier Rodríguez-Tovar^g, Javier Dorador^h, Stéphanie Desprat^{a,b}

^a Ecole Pratique des Hautes Etudes (EPHE, PSL University), F-33615 Pessac, France

^b University of Bordeaux, EPOC, UMR 5805, F-33615 Pessac, France

^c Dipartimento di Scienze Ambientali, Informatica e Statistica, Università Ca' Foscari Venezia, Venice I-30172, Italy

^d Basque Centre for Climate Change – BC3, Sede Building 1, 1st floor, Scientific Campus of the University of the Basque Country, 48940 Leioa, Spain

^e Divisão de Geologia e Georecursos Marinhos, Instituto Português do Mar e da Atmosfera, Rua Alfredo Magalhães Ramalho, 6, 1495-006 Lisboa, Portugal

^f Centro de Ciências do Mar (CCMAR), Universidade do Algarve, Campus de Gambelas, 8005-139 Faro, Portugal

^g Departamento de Estratigrafía y Paleontología, Universidad de Granada, Avda. Fuentenueva s/n, 18002 Granada, Spain

^h Department of Earth Sciences, Royal Holloway University of London, Egham, Surrey TW20 0EX, UK

ARTICLE INFO

Article history:

Received 21 June 2018

Received in revised form 10 January 2019

Accepted 18 January 2019

Available online xxxx

Editor: R. Pancost

Keywords:

Mid-Pleistocene Transition

southwestern Europe

pollen

vegetation

precipitation

temperature

ABSTRACT

The MIS 17 interglacial, ~715–675 ka, marks the end of the Mid-Pleistocene Transition as intensified, long and asymmetrical 100-kyr ice age cycles became eminently established. Increasing arrival of moisture to the Northern Hemisphere high latitudes, resulting from the northwestward migration of the Subpolar Front and the intensification of the Norwegian Greenland Seas (NGS) convection, has been put forward to explain the emergence of this quasi-periodic 100-kyr cycle. However, testing this hypothesis is problematic with the available North Atlantic precipitation data. Here we present new pollen-based quantitative seasonal climate reconstructions from the southwestern Iberian margin that track changes in the position and intensity of the westerlies. Our data compared to changes in North Atlantic deep and surface water conditions show that MIS 17 interglacial was marked by three major changes in the direction and strength of the westerlies tightly linked to oceanographic changes. In particular, we report here for the first time a drastic two-steps northward shift of the westerlies centered at ~693 ka that ended up with the sustained precipitation over southern European. This atmospheric reorganization was associated with northwestward migration of the Subpolar Front, strengthening of the NGS deep water formation and cooling of the western North Atlantic region. This finding points to the substantial arrival of moisture to the Northern Hemisphere high latitudes at the time of the decrease in summer energy and insolation contributing to the establishment of strong 100-kyr cycles.

© 2019 Elsevier B.V. All rights reserved.

1. Introduction

The Marine Isotopic Stage (MIS) 17 interglacial, ~715,000–675,000 yr ago (715–675 ka), preceded the onset of the firmly established 100-kyr ice age cycles at ~650 ka (MIS 16) (Baher et al., 2018; Elderfield et al., 2012; Hodell and Channell, 2016; Mudelsee and Stettger, 1997; Wright and Flower, 2002). Both,

proxy data (Ehlers and Gibbard, 2007; Hodell et al., 2008; Naafs et al., 2013) and model simulations (Bintanja and van de Wal, 2008) suggest that the North American ice sheets surpassed the Eurasian ice masses to become the dominant ice accumulations of the Northern Hemisphere. This switch to greater ice accumulation in North America coincided with a major reorganization of both surface and deep North Atlantic oceanic currents when the “Boreal heat pump” was replaced by the “Nordic heat pump” implying a northwest migration of the Subpolar Front (Alonso-García et al., 2011; Imbrie et al., 1993; Wright and Flower, 2002) and the intensification of the North Atlantic deep water formation (Poirier and Billups, 2014). This hypothesis assigns a key role to the “Nordic heat pump” in establishing the strong

* Corresponding author at: Ecole Pratique des Hautes Etudes (EPHE, PSL University), UMR EPOC, University of Bordeaux, Allée Geoffroy St Hilaire, 33615 Pessac, France.

E-mail address: maria.sanchez-goni@u-bordeaux.fr (M.F. Sánchez Goñi).

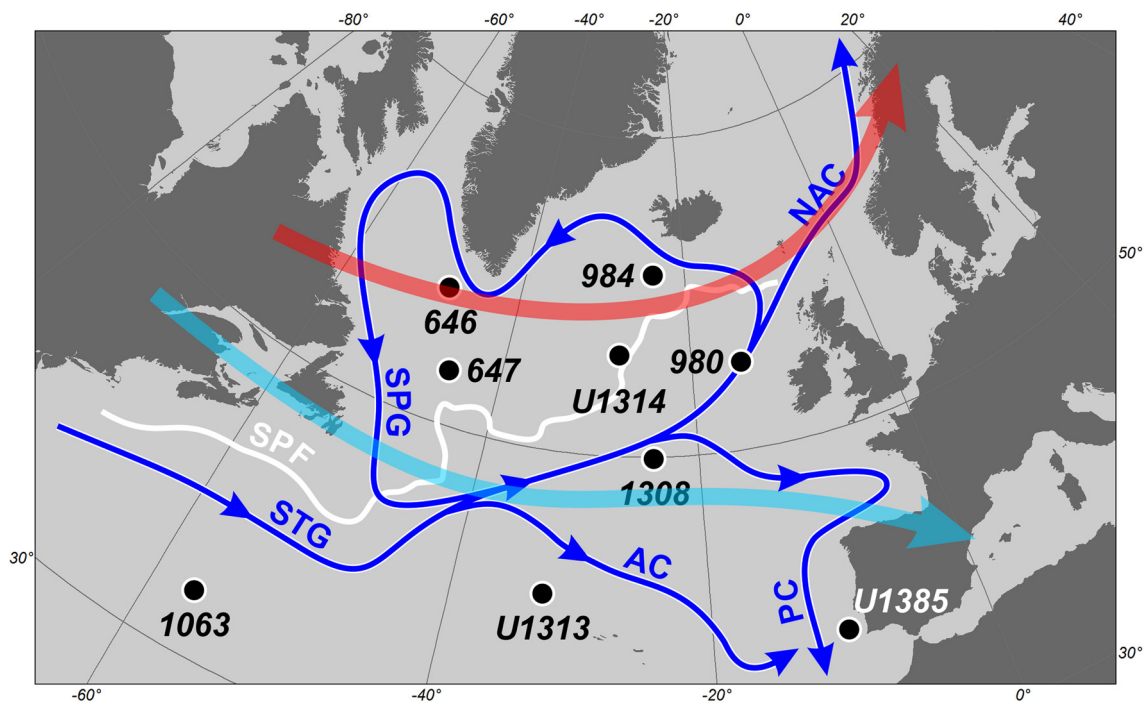


Fig. 1. Map with the sites discussed in the text. The position of the present-day Subpolar Front follows approximately the 10°C isotherm (Marchal et al., 2016). STG: Subtropical gyre; AZ: Azores Current; PC: Portuguese Current; SPG: Subpolar gyre; NC: Norwegian Current. Red and blue arrows indicate the northward and zonal path of the westerlies, respectively. (For interpretation of the colors in the figure(s), the reader is referred to the web version of this article.)

100-kyr cyclicity of the late Pleistocene glacial cycles because it enhanced the moisture transport to the northern high latitudes that promoted ice sheets build-up. Likewise, deep water formation mainly occurred in the Subpolar North Atlantic before 700 ka causing reduced poleward heat transport (Imbrie et al., 1993; Wright and Flower, 2002). Well-established 100-kyr cycles would therefore have been started by a change between a long period of advection of warm water that enhanced moisture transport to southern Europe and the growth of Alpine glaciers (Bahr et al., 2018) and a period of a decreasing trend in the sea surface temperature (SST) east-west gradient (Alonso-García et al., 2011; Wright and Flower, 2002) associated with the northward shift of the westerlies that brought warmth and precipitations to northern Europe. However, no data exists so far demonstrating the sustained arrival of high amounts of moisture to southern Europe during MIS 17 and the subsequent northward shift of precipitation to colder regions of the Northern Hemisphere feeding the ice caps.

Here we present the first record of atmospherically-driven vegetation dynamics in southwestern Europe during the MIS 17 interglacial testing if the reconfiguration of oceanic and atmospheric circulation during MIS 17 might have preconditioned enhanced ice sheet growth during MIS 16. We analyzed the pollen preserved in the southwestern Iberian margin IODP site U1385 (Fig. 1) to infer regional vegetation changes and quantitatively reconstruct seasonal and annual temperatures and precipitation. The westerlies are responsible for most of the precipitation arriving in Europe (Brayshaw et al., 2010) and the main factor currently controlling vegetation greenness, an indicator of forest cover, in the Iberian Peninsula (Gouveia et al., 2008). This direct relationship between westerlies and forest cover in Iberia makes pollen-inferred forest cover changes recorded in the U1385 sedimentary record be ideally suited to track past shifts in the position of the westerlies. We performed numerical zonation and time series analyses (change point method and Fourier and wavelet spectral analysis) on the Mediterranean forest pollen record to identify significant changes in the vegetation and therefore in the westerlies, and the dominant cyclicities. Changes in the type and rate of sedimentation

based on ichnofabric analysis provide additional information on major shifts in local deep water conditions. Our vegetation-based westerlies record was then compared with changes in $\delta^{18}\text{O}$ of benthic foraminifera ($\delta^{18}\text{O}_b$) (Hodell and Channell, 2016; Hodell et al., 2015) and sea surface conditions from the same site (Bahr et al., 2018; Martín-García et al., 2015; Rodrigues et al., 2017), and with other North Atlantic records of surface and deep ocean changes documented further north and west (Alonso-García et al., 2011; Naafs et al., 2013; Poirier and Billups, 2014; Wright and Flower, 2002) (Fig. 1).

2. Present-day environmental setting

IODP Site U1385 (37°34.285'N, 10°7.562'W, 2578 m depth) is located on a spur, the Promontorio dos Príncipes de Avis. The sedimentary section recovered at Site U1385 (1.5 km-long record) shows hemipelagic continental margin sediments deposited under normal marine conditions with a fully oxygenated water column and average sedimentation rates of 10 cm/ky (Stow et al., 2013). The surface water column at the site is affected by the Portuguese current (PC) which brings cold nutrient-rich water from the northern latitudes and forms the Eastern North Atlantic Central Waters of subpolar origin (ENACWsp), and by the Azores current (AC) which brings warm water from the Azores front generating the ENACW of subtropical origin (ENACWst) (Ríos et al., 1992). ENACWsp underlies the ENACWst and form the permanent thermocline down to c. 500 m water depth (Fig. 1).

The present-day climate of southwestern Iberia, 1961–1990 period, is Mediterranean with warm and dry summers and mild and wet winters. During winter the North Atlantic westerlies bring moisture to the Iberian margin (Fig. 1), while a high pressure cell develops in the North Atlantic during summer, which generates strong northerly trade winds inducing coastal upwelling (Fiúza et al., 1982). The mean winter (DJF) and summer (JJA) precipitation is 250 and less than 50 mm, respectively (80 and <20 mm/month) (Miranda et al., 2002); mean winter and summer temperatures are at around 10°C and 22°C, respectively (Ramos et al., 2011). This

strong seasonality lead to the development of a Mediterranean vegetation in the adjacent landmasses dominated by deciduous oak at middle elevation (700–1000 m a.s.l.), and evergreen oak, olive tree, *Pistacia*, *Phillyrea* and rockroses (*Cistus*) at lower elevations (Blanco Castro et al., 1997).

3. Material and methods

3.1. Stratigraphy and age model

The stratigraphy of Site U1385 was built upon a combination of chemo-stratigraphic proxies (Hodell et al., 2015). Ca/Ti ratio measured every cm in all holes by core scanning XRF was used to construct a composite section, and low resolution (20 cm) oxygen isotopes of benthic foraminifera ($\delta^{18}\text{O}_b$). For consistency with previous works from the same site (Sánchez Goñi et al., 2016), the age model of the studied interval was based, among the two age models proposed by Hodell et al. (2015), on the correlation of the $\delta^{18}\text{O}_b$ record to the marine $\delta^{18}\text{O}_b$ stack of LR04 (Lisiecki and Raymo, 2005) (Table 1).

3.2. Pollen analysis and quantitative climatic reconstruction

Sediment subsamples 1-cm thick and 2.5–4 cm³ volume were prepared for pollen analysis using an optimized protocol for marine samples, <http://www.ephe-paleoclimat.com/Files/Other/Pollen%20extraction%20protocol.pdf>, employing coarse-sieving at 150 μm , successive treatments with cold HCl, cold HF at increasing concentration and micro-sieving (10 μm mesh). At the beginning of the treatment, we added known quantities of *Lycopodium* spores in tablet form to calculate pollen concentration. Slides were prepared using a mobile mounting medium, i.e. glycerol, to permit rotation of the pollen grains and a transmitted Primo Star light microscope was used for routine identification of pollen and spores at 400 \times and 1000 \times magnifications. One hundred samples were analyzed every 4 cm in average. Excluding ten samples with pollen counts between 50 and 100, pollen counts oscillate between 100 and 166 terrestrial pollen grains excluding *Pinus*, aquatics and spores (total sporo-pollen sum between 117 and 754). The number of pollen morphotypes in most of the samples, 78 samples out from 100, ranges from 20 to 27, and from 13 to 19 morphotypes in the remaining samples. Pollen percentages for terrestrial taxa were calculated against the main sum of terrestrial grains, while percentages for *Pinus* were calculated against the main sum plus *Pinus*. Aquatic pollen and spores percentages are based on the total sum (Pollen + spores + indeterminables + unknowns). We assume that the average uncertainty of the calculated pollen percentage values in our analysis is less than 8%, based on the average error of 7.9% calculated by Fletcher and Sanchez Goñi (2008). Total sporo-pollen concentrations oscillate between 9000 and 147,000 grains-cm⁻³ (Fig. S1). Changes in grain concentrations do not parallel changes in pollen percentages and, therefore, these latter changes indicate actual variations in forest cover and composition. However, one should keep in mind that the relationship between arboreal pollen percentages and forest cover is not direct, which is mostly due to the difficulty of estimating the role of all the different factors influencing the palynological data (e.g. pollen productivity and dispersability, source area and distance to sample site, amenability to wind dispersal, deposition and preservation until sampling and analysis of vegetation dynamics) (e.g. Bradshaw and Webb, 1985). Nevertheless, this does not affect our pollen-vegetation relationships as previous work has shown that the pollen percentage variations reflect the past forest cover patterns (Williams and Jackson, 2003) and vegetation composition (Nieto-Lugilde et al., 2015).

The interpretation of the pollen diagram was assisted by a constrained hierarchical clustering analysis (CONISS) based on Euclidean distance between samples and applied to the total pollen counting. Analysis was performed in the R environment v. 2.13.2 (R Development Core, 2011) using the `chclust` function from package *Rioja* (Juggins, 2009).

We reconstructed paleoclimate for each pollen sample using a Plant Functional Type (PFT) Modern Analogue Technique (MAT) (Mauri et al., 2015) implemented in the R package 'Rioja' (Juggins, 2012). The Modern Analogue Technique (MAT) is considered the most suitable method for large-scale climate reconstructions from terrestrial and marine pollen sequences, especially when the training set encompasses a wide range of vegetation and climate zones (Brewer et al., 2007; Juggins and Birks, 2011). In this case, we complied with this assumption using the extensive European Modern Pollen Database (Davis et al., 2013). We reconstructed a range of climate parameters usually estimated from pollen data, namely mean monthly summer (JJA), winter (DJF) and annual temperature and precipitation.

3.3. Ichnological research

This research was based on digital image analysis treatment (Dorador and Rodríguez-Tovar, 2018), on selected cores of IODP Site U1385. The technique is based on image adjustment modifications to enhance ichnoassemblage visualization and characterization. Three adjustment modifications (*levels*, *brightness* and *vibrance*) were applied to the high-resolution images using Adobe Photoshop CS6 software[®] for enhancing the visibility of biogenic structures. Ichnotaxonomic identification is mainly based in ichnological observations achieved from cores (Knaust, 2017). In each of these images, ichnofabric attributes (i.e., ichnoassemblage, cross-cutting relationships and degree of bioturbation) are characterized. Quantitative estimation on the percentage of bioturbation was obtained by the application of the Ichnological Digital Analysis Images Package (Dorador and Rodríguez-Tovar, 2018). The amount of bioturbation was characterized and referred to the Bioturbation Index (Taylor and Goldring, 1993).

3.4. Time series analyses

We used REDFIT (Schulz and Mudelsee, 2002) to estimate the Fourier spectrum directly from the unevenly spaced time series of the Mediterranean forest pollen percentages, and we removed the linear trend before estimating the spectrum. One of the main advantages of REDFIT is that this method is able to separate real signals from the red noise background. To explore potential climate regime shifts contained in the paleoclimate data under analysis, we used the change point method proposed by Bai and Perron (2003), as implemented in the R package `strucchange` (Zeileis et al., 2002). This statistical tool identifies the age where there exists a significant structural change in the times series analyzed providing the 95% CI (confidence interval) of the change-point, but this tool works only with evenly spaced ("regular") time series. For this reason, we interpolated the unevenly spaced time series of pollen percentages through Akima method using intervals of 200 yr. Furthermore, others interval lengths ("100" and "300" yr) were used, but the results did not change and are not shown. To estimate the wavelet spectrum to the interpolated pollen percentages (using the same preprocessing strategy such as was described previously) via the Morlet continuous wavelet transform we used the method of Liu et al. (2007), as implemented in the R package `biwavelet` (Gouhier and Grinsted, 2014). Please note that it is not necessary to remove a linear trend in the time series of pollen percentages because wavelet spectral analysis is designed to work with non-stationary time series.

Table 1

Control points used to establish by linear interpolation the age model of the interval MIS 17 in IODP Site U1385. The age model is based on the LR04 stack (Lisiecki and Raymo, 2005).

Depth (cmcd)	Age ka (LR04)	Sedimentation rate (cm/kyr)	Hole
79.43	662.31	7.05	D
80.79	686.37	5.65	D
81.83	696.67	10.09	D
84.10	719.49	9.93	A

4. Results

4.1. From pollen-based vegetation changes to westerlies shifts

The studied section of U1385 spans the period between 715.2 ka and 672 ka, encompassing the very end of MIS 18, the 38-kyr long MIS 17 (713–675 ka), and the very beginning of MIS 16 (Hodell et al., 2015). The sedimentation rate varies between 5.65 and 10.09 cm/kyr (Table 1) and the temporal resolution of the pollen analysis is 380-year on average. Pollen diagrams show (Figs. 2 and 3e) a long-term increase of the Mediterranean forest pollen percentages, mainly composed of deciduous *Quercus* and sclerophyllous taxa (evergreen *Quercus*, *Olea*, *Cistus*, *Pistacia* and *Phillyrea*) that tightly follows the gradual changes in summer energy at 65°N (Fig. 3a), defined as the number of summer days in which daily insolation is above 275 W/m² (Huybers, 2006). This parameter integrates the duration and intensity of insolation during the summertime and it is mainly paced by obliquity (Huybers, 2006). Throughout the MIS 17 interglacial, low percentages of sclerophyllous trees and shrubs point to the occurrence of weakly Mediterranean climate compared with other interglacials (Sánchez Goñi et al., 2018), indicating limited seasonality. The two maxima in sclerophyllous plants reveal increased summer warmth and dryness but still high winter precipitation during MIS 17e (~712 ka) and 17c (694 ka) (Fig. 3b and e) and coincide with the two minima in precession that determine stronger seasonality (Meijer and Tuenter, 2007) (Fig. 3a). The terrestrial counterpart of the MIS 17 interglacial *sensu stricto* lasted 27 kyrs (~714–687 ka) in southwestern Iberia according to the criterion used in previous research at the same site (Mediterranean forest pollen >20%; Sánchez Goñi et al., 2016). It was followed by a significant forest contraction during MIS 17b and a subsequent forest increase during MIS 17a (~678–673 ka). Superimposed to these orbitally-driven Mediterranean forest changes, time series analyses suggest a succession of forest contractions with dominant 5.2-kyr (90%) and 1-kyr (95%) cyclicities (Figs. 3e, 4 and 5). Quantitative reconstructions of average seasonal and annual temperature and precipitation show a long-term trend characterized by higher winter precipitation during MIS 17e, d and c with a decrease during the second part of this interglacial, MIS 17b and a. During MIS 17c, summer temperature and precipitation records reveal the highest and lowest values, respectively. We recognize that the uncertainties of our quantitative climatic estimations are large, particularly those of winter precipitation, and this is certainly due to the lack of good modern pollen analogues for the MIS 17 interglacial. However, our pollen-based quantitative estimations are in line with present-day vegetation requirements and atmospheric circulation (Gouveia et al., 2008) and, therefore, with our qualitative interpretation. Moreover, in a recent paper (Oliveira et al., 2018) we have clearly shown using a data-model comparison approach that the Mediterranean forest pollen percentage and tree fraction have a strong relationship with winter precipitation.

Constrained hierarchical cluster analysis reveals four main pollen zones (Figs. 2 and 3). The first zone, U1385-1 (~715.2–714 ka, MIS 18), falls within the Termination VIII, and is marked

by the highest semi-desert pollen percentages (mainly *Artemisia*, *Chenopodiaceae* and *Ephedra*), indicating that winters were particularly cold and dry with precipitation below present-day values (Fig. 6d and e). The onset of the next pollen zone, U1385-2 (~714–700 ka, MIS 17e–d) is marked by the large and rapid increase of *Ericaceae* and Mediterranean forest taxa (mainly deciduous *Quercus*, <10%–30%), within 400 yr. Today, *Ericaceae* are abundant in Europe under relatively moist climates with more than 600 mm of annual precipitation, low seasonality, and at least four months of mean temperatures above 10 °C (Polunin and Walters, 1985). Our climatic reconstruction indicates a rapid shift to more humid (20 mm/month winter and summer increases compared to the previous zone) but still cool conditions (3 °C and 19 °C in winter and summer, respectively) at ~713 ka (Fig. 6b–e). *Ericaceae*-dominated shrublands (heathlands) reached its maximum expansion at ~710 ka associated with a moderate increase of deciduous trees and sclerophyllous plants pointing to maximum summer precipitation (up to 50 mm/month, i.e. 30 mm/month more than at present) by that time (Figs. 3d, e and 6c). The significant increase of the Mediterranean forest cover at ~707 ka (Fig. 2), corroborated by the change point method (Fig. S2), indicates a first winter and summer warming (Fig. 6b and e). Summer precipitation remained higher than at present for 15,000 yr but winter precipitations slightly decreased. High winter and summer precipitation and moderate warmth during the interval MIS 17e–d (Fig. 6b–e) probably resulted from well-developed Eurasian ice caps (Bintanja and van de Wal, 2008; Hodell et al., 2008). This ice configuration maintained the westerlies and, therefore, precipitation in a southern position comparable, albeit with lesser intensity due to less ice volume, to what is observed and simulated during the last glacial maximum in southern Europe (Lainé et al., 2009; Prentice et al., 1992). A similar heathlands expansion, although with less forest cover, is observed during the last glacial maximum in this region (Turon et al., 2003).

At the beginning of pollen zone U1385-3 (~700–692 ka, MIS 17c), Mediterranean forest (>40%; deciduous *Quercus* >30%) replaced heathlands (<15%) (Figs. 2 and 3e), reaching a maximum (up to 78%) at ~696 ka. Modern pollen studies indicate oak forest dominance and heathland presence when deciduous *Quercus* and *Ericaceae* pollen percentages are above 30% and below 25%, respectively (Huntley and Birks, 1983; Sánchez Goñi and Hannon, 1999). Heathland-dominated landscapes during MIS 17e–d were therefore progressively replaced by the Mediterranean forest. Longer growing seasons favor the development of broad-leaved trees (Kollas et al., 2014) and this particular vegetation change indicates that spring-winter mean temperature progressively increase. This lengthening of the growing season parallels the increase in summer duration, peaking at ~696 ka (Fig. 6a). This interval between ~696 and 694 ka is characterized by the highest mean summer temperatures reaching almost present-day values (22 °C, Fig. 6b). Furthermore, mean winter precipitation estimations show that rainfall increased and was again higher than that of the present day. MIS 17c was therefore the period characterized by both maximum summer warmth and dryness and strong influence of the westerlies in this region. It coincides with a strong expansion of the temperate forest in southern Italy (tree pollen percentages of 80%, Montalbano Jonico, 40°17'N) (Toti, 2015) suggesting that the westerlies substantially affected more eastern and northern regions. A first sharp decrease of the Mediterranean forest in the adjacent landmasses at ~694 ka, pollen percentages from 78% to 60% during the transition MIS 17c/17b, suggests a decrease in winter precipitation, which went under present-day values (Fig. 6e). This shift corresponds with slightly decreasing winter temperatures but still warm summers (Fig. 6d and b). Colder and drier winter conditions compared with MIS 17c suggest a northward shift of the westerlies and their weaker influence in southern Europe at the time of sea

U1385-MIS 17

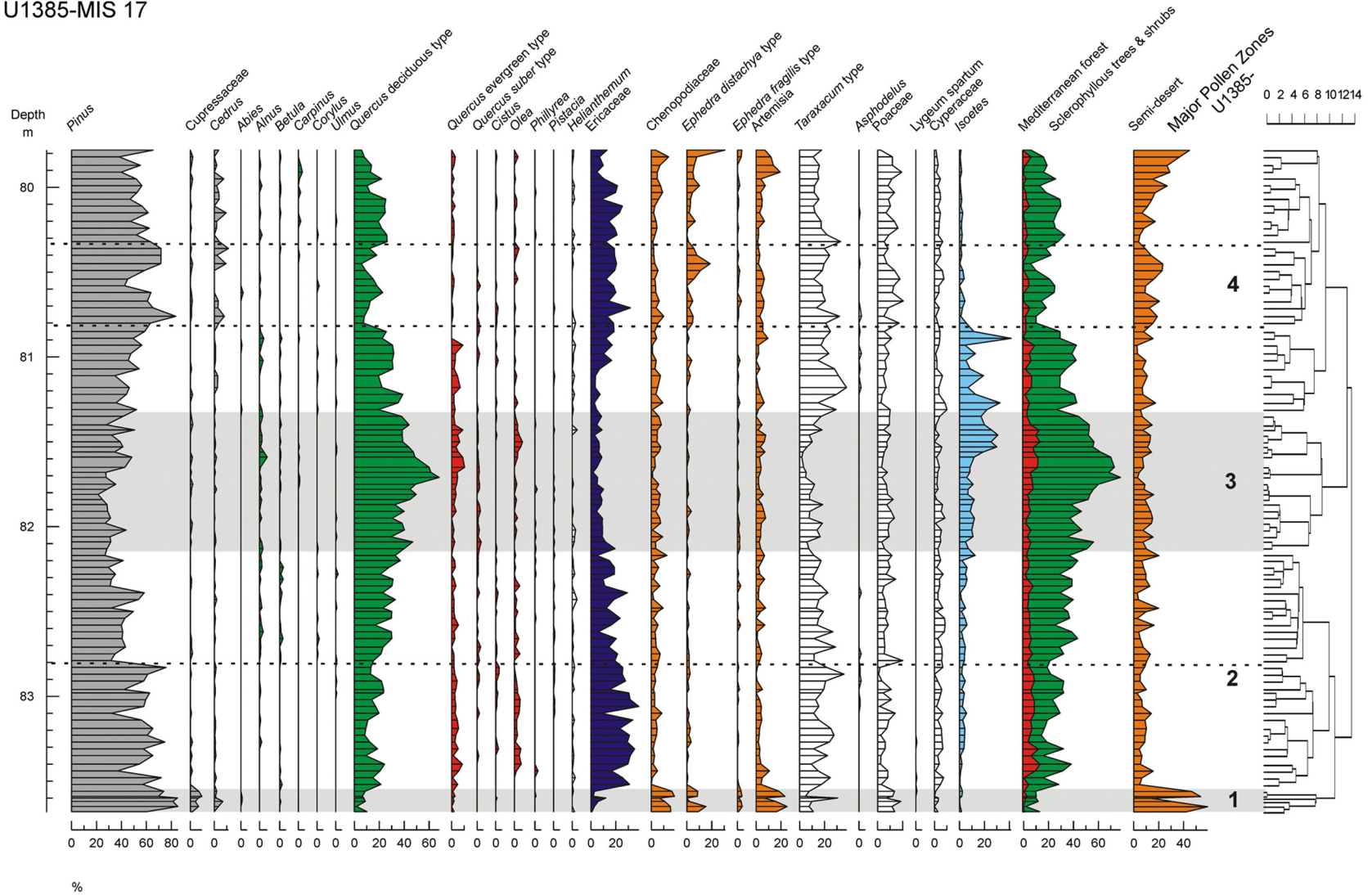


Fig. 2. Detailed pollen diagram with selected taxa and ecological groups. On the right side we show the four main pollen zones identified by the constrained hierarchical cluster analysis (CONISS). (For interpretation of the colors in the figure(s), the reader is referred to the web version of this article.)

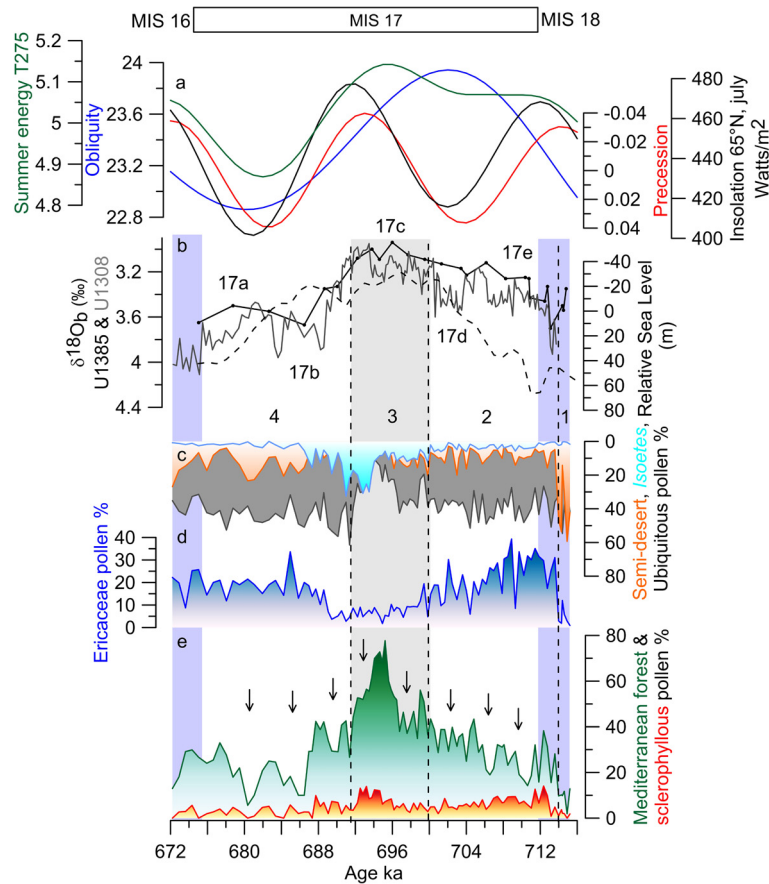


Fig. 3. Pollen-inferred vegetation changes during MIS 17 in southwestern Iberia, along with changes in ice volume and orbital forcing: (a) Summer energy (green line), T275 defines the number of summer days in which daily insolation is above 275 W/m^2 (Huybers, 2006), July insolation at 65°N (black line), precession index (red line) and obliquity (blue line) (Berger and Loutre, 1991). (b) Low and high resolution $\delta^{18}\text{O}_b$ profiles from IODP sites U1385 (black line) (Hodell et al., 2015) and U1308 (grey line) (Hodell and Channell, 2016) respectively, and relative sea level curve (stippled line) (Elderfield et al., 2012). (c–e) Pollen percentages of the most relevant plant taxa and ecological groups (IODP site U1385). The position of MIS 17a–e sub-stages follows Railsback et al. (2015). Numbers 1 to 4 indicate the four main pollen zones. Dashed lines indicate the significant onset of the major pollen zones. Long arrows in panel (e) depict the 5.2-kyr cyclicity of forest contractions. Grey bar represents the interval with the maximum development of the Mediterranean forest. Blue bars denote MIS 18 and MIS 16. (For interpretation of the colors in the figure(s), the reader is referred to the web version of this article.)

level decreasing trend (Fig. 3b). An alternative hypothesis involving a decrease in the amount of moisture transported by the westerlies brought about by the cooling of the subtropical gyre could also explain the dryness recorded at the end of MIS 17c. However, as we will see later, the decrease in the Mediterranean forest and related winter precipitation occurred when the SST in the Iberian margin were still high, between 18 and 20°C . The abundance of *Isoetes* spores notably increased by that time, probably expanding in temporary wetlands established on the coastal areas emerged (Salvo Tierra, 1990) during the contemporary sea level fall.

The last pollen zone, U1385-4, encompasses MIS 17b, MIS 17a and the beginning of MIS 16 (~ 692 – 673 ka). Its onset is marked by a second sharp decrease of Mediterranean forest pollen (30–40%) at ~ 692 ka, corroborated by the change point analysis (Fig. S2). Ubiquitous herbs largely increased, inferring a winter climate 2°C colder and 10 mm/month drier compared to pollen zone U1385-3 probably amplified by the decrease in summer insolation that follows the decrease in summer energy (Figs. 3c and 6a, d, e). Colder and drier winters in southwestern Iberia suggest a further northward displacement of the westerlies. The second part of this pollen zone, ~ 686 – 673 ka, is additionally marked by the increase of heathlands and semi-desert plants and the lowest Mediterranean forest cover of MIS 17 (Fig. 3). These data reveal relatively wet summers, dry winters and a cooler climate during MIS 17b–a (Fig. 6b–e) and we infer a still weaker influence of the westerlies

in southwestern Iberia likely related to their sustained northward penetration at the time of ice growth.

4.2. Local bottom water oxygenation

Trace fossils, as reflecting behavior of trace makers, provide detailed information on ecological and depositional parameters; especially, archetypal ichnofacies, as group of biogenic structures that reflect animal responses to paleoenvironmental conditions (MacEachern et al., 2012). Trace fossil assemblage through the studied interval consists of *Planolites* (*Pl*), *Thalassinoides* (*Th*), *Thalassinoides*-like (*Th*-1) structures, and *Zoophycos* (*Zo*) that can be ascribed to the *Zoophycos* ichnofacies, typical of deep sea environments (Figs. 7 and S3). These discrete traces are overlapping a mottled background, Bioturbation Index (BI) of 6, associated with biodeformational structures. Abundance of these discrete trace fossils is variable with BI ranging from 1 to 4 (Fig. 7). On this general pattern, significant stratigraphical changes can be observed, allowing differentiation of four ichnofacies: *Thalassinoides*-like ichnofabric, characterized by dominant *Th*-1, and the presence of *Pl* and *Th*; *Planolites* ichnofacies, with dominance, near exclusiveness of *Pl*, and light host sediment, *Zoophycos* ichnofabric, with dominant *Zo* and some *Th*, and darker host sediment; and *Thalassinoides* ichnofabric, with dominance of *Th*, and the record of *Pl*. Especially significant is the change between the *Planolites* ichnofabric and the *Zoophycos* ichnofabric at

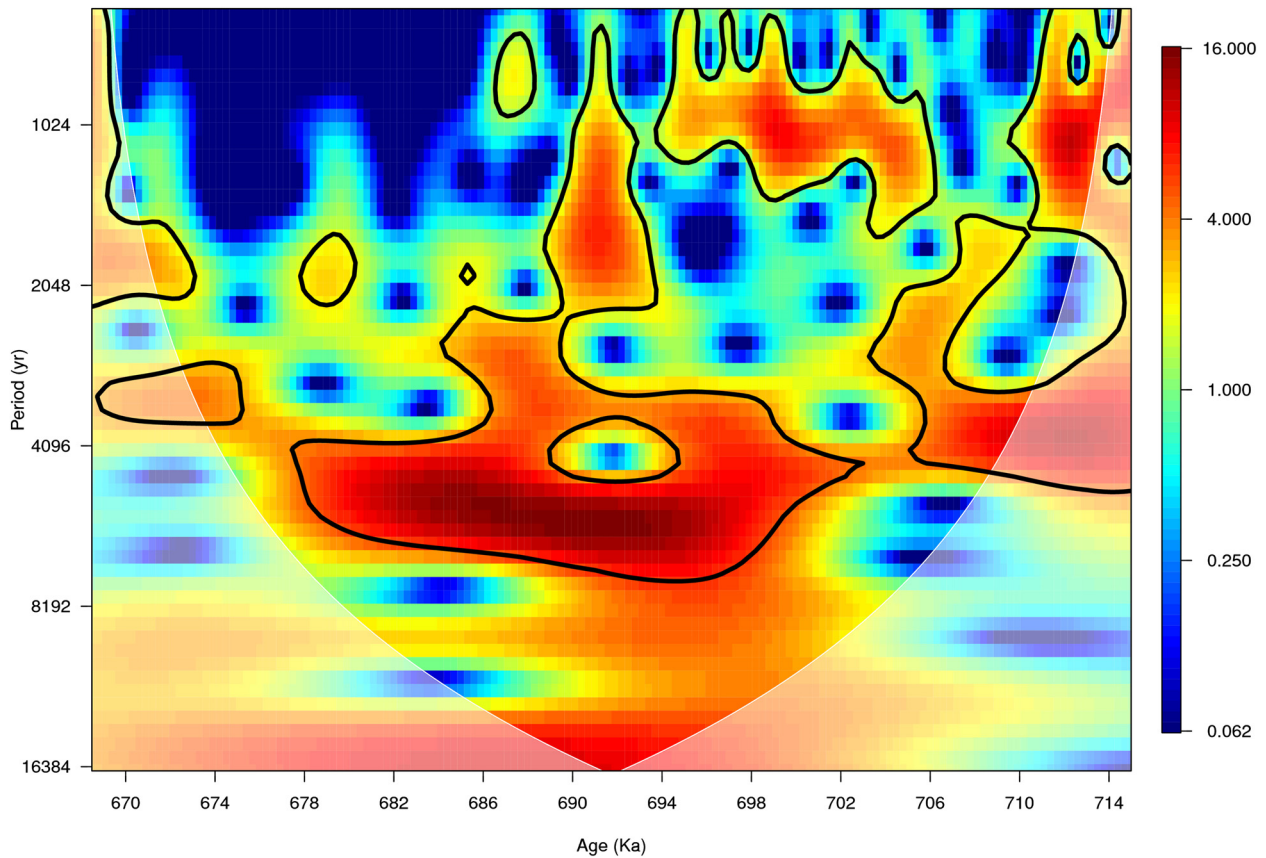


Fig. 4. Wavelet spectrum via the Morlet continuous wavelet transform computed for the time series of Mediterranean forest pollen percentages. A strong signal around 5,000-yr dominates a large part of the MIS 17 interglacial. The solid black contour encloses regions of $\geq 80\%$ confidence. (For interpretation of the colors in the figure(s), the reader is referred to the web version of this article.)

81.43 m, centered at ~ 693 ka. Dominant/exclusive *Planolites* over a mottled background has been previously interpreted for IODP Site U1385 as bioturbation of uppermost tiers, on or just below the seafloor, associated with relatively good life conditions for macrobenthic trace maker community (oxygenation and nutrients availability) (Rodríguez-Tovar and Dorador, 2014). In this context, absence of deeper tier traces could reveal a relatively high sedimentation rate which avoids the colonization deeper into the sediment. The abrupt appearance of *Zoophycos*, together with *Thalassinoides*, evidences colonization of deeper tiers; this could be related with decreasing in the rate of sedimentation, determining enough time for bioturbation and colonization deeper in the sediment. This time is necessary for development of complex structures such as *Zoophycos*. *Zoophycos* producer has been related to variations in energy, sedimentation rate, food content, or bottom-water oxygenation (Dorador et al., 2016); its relative independence of substrate features would allow for colonization of sediments with comparative low oxygenation (Rodríguez-Tovar and Uchman, 2008). *Zoophycos* is commonly found in hemipelagic sediments deposited during glacial times and when the sedimentation rate was intermediate (from 5 to 20 cm kyr^{-1}) and primary production was high and seasonal (Dorador et al., 2016). Occurrences of *Zoophycos* elsewhere support a similar relationship with seasonal organic-matter deposition. Thus, in the case study, the record of the *Zoophycos* ichnofabric could be related with changes in primary productivity and decreasing in the rate of oxygenation, also supported by the darker color of the sediment, in a context of higher sedimentation rate. The lightness record from the same IODP site U1385 also shows a substantial change towards higher values in the *Zoophycos* interval (Fig. 7)

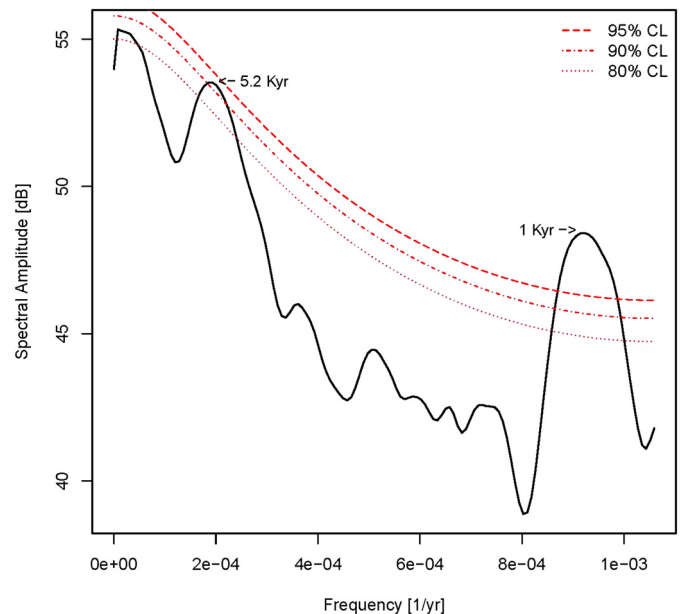


Fig. 5. Spectral analysis based on REDFIT. This analysis identifies two dominant cyclicities, at 5,200 yr (90%) and at 1,000 yr (95%).

(Hodell et al., 2013). This strong lightness found in darker sediments could be explained by the abundant bioturbation characterizing this zone and introducing light material in a dark sediment background.

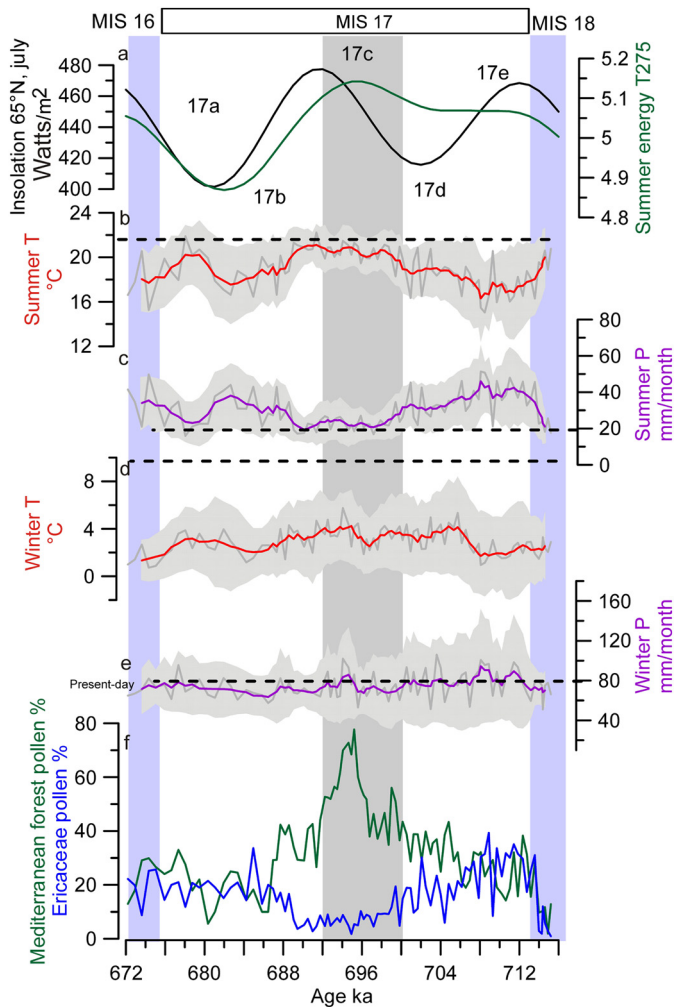


Fig. 6. Pollen-based quantitative climatic reconstructions for southwestern Europe during MIS 17 and orbital forcing: (a) Summer energy (green line) (Huybers, 2006), July insolation at 65°N (black line) (Berger and Loutre, 1991). (b–d) Summer, June–August, and winter, December–February, temperature reconstructions (dark grey), and 5-point weighted average curve (red). (c–e) Summer, June–August, and winter, December–February, precipitation reconstructions (dark grey) and 5-point weighted average curve (purple). (f) Pollen percentages of Mediterranean forest (mainly deciduous and evergreen *Quercus*, *Olea*, *Pistacia*, *Phillyrea*, *Cistus*) and Ericaceae. Grey shadow indicates the minimum and maximum standard errors that are the uncertainties calculated by the transfer function (Mauri et al., 2015). Dashed lines are present-day (1961–1990) temperature and precipitation from southwest Portugal (Miranda et al., 2002; Ramos et al., 2011). Blue bands show MIS 16 and MIS 18 glacial periods. Grey band represents the pollen zone U1385–3. The position of MIS 17a–e sub-stages follows Railsback et al. (2015). Present-day climate refers to the 1961–1990 period. (For interpretation of the colors in the figure(s), the reader is referred to the web version of this article.)

5. Discussion

Vegetation-inferred shifts in the westerlies and in local bottom water oxygenation during MIS 17 were compared with sea surface changes in southwestern Iberian margin and other North Atlantic paleoceanographic records located west in the subpolar gyre (ODP Sites 646 and 647; IODP Site U1314; ODP Site 984), in the mid-latitude central North Atlantic (IODP Site U1313) and in its easternmost part, off Ireland (ODP Site 980, Fig. 1). Reduced precipitation at the end of MIS 18 was synchronous with $\delta^{13}C_{37:4}$ -based freshwater pulses and the lowest UK $_{37}$ -SST in the southwestern Iberian margin (Rodrigues et al., 2017) (Fig. 8e and f), as well as the presence of ice rafted debris (IRD) in the subpolar gyre (Alonso-Garcia et al., 2011) indicating that the Subpolar Front and the associated storm tracks (Ogawa et al., 2012), were

located at the mid-latitudes of the Iberian margin as far south as below 37°N (Rodrigues et al., 2017) (Fig. 9). The subsequent 15-kyr long period of sustained summer and winter wetness and annual cool climate between ~713 ka and 700 ka, was associated with warm waters off southwest Iberia, as indicated by UK $_{37}$ and foraminifera-based SST records from the same site (Martin-Garcia et al., 2015; Rodrigues et al., 2017). During this time interval SSTs in the subpolar-central North Atlantic (U1314) (Alonso-Garcia et al., 2011) and in the western mid-latitude basin (U1313) (Naafs et al., 2011) were the highest of the records and higher than the SST in the northeastern part (ODP 980) (Fig. 8c and Fig. S4). This gradient suggests a westward location of the Subpolar Front and deep water formation sites (Alonso-Garcia et al., 2011; Wright and Flower, 2002). The relatively small thermal gradient during the interval from 700 ka to 692 ka between the southern Mg/Ca-based thermocline temperature on *Globorotalia inflata* (U1385, 37°N) and the slightly northern alkenone-based SST record (U1313, 41°N) (Fig. 8d) additionally suggests a southward position of the thermocline water source of the ENACWsp (Bahr et al., 2018) (Fig. 9). The high amount of winter and summer precipitation in southwestern Europe during MIS 17e–d in comparison with the end of MIS 18 suggests a mid-latitude position of the westerlies during winter and enhanced moisture production during summer giving support to the relative southern position of this warm source region (Bahr et al., 2018) (Fig. 9). Moreover, the dominant 5.2-kyr cyclicity in the Mediterranean forest pollen percentage changes recorded during MIS 17e–d–c in the absence of high latitude ice-related freshwater pulses (Alonso-Garcia et al., 2011) (Figs. 4, 5 and 8f) call to the fourth harmonic of precession, i.e. the influence of tropical regions on southwestern Iberian climate (Sánchez Goñi et al., 2016). The reason why low latitudes may lead to millennial-scale changes is due to the fact that they receive, with respect to higher latitudes, twice the maximum amount of daily irradiation over the course of the year (Berger et al., 2006). A direct consequence of this process would be a larger latitudinal thermal gradient and thus enhanced transport of warmth and moisture by either atmospheric (westerlies) or oceanic circulation (subtropical gyre) from equatorial to high latitudes in the North Atlantic (Berger et al., 2006). The arrival of precipitation during winter to a cool Europe allowed the Alpine glaciers, which strongly developed during the 0.8–1.0 Ma time interval (Haeuselmann et al., 2007; Valla et al., 2011), to persist.

At the MIS 17d/c transition, centered at ~700 ka, southwestern Iberia warmed up and winter precipitation decreased followed by a sharp increase alongside increasing summer energy (Figs. 5a, f and 7a, g). Bahr et al. (2018) suggested that the thermocline water source of the ENACWsp moved progressively northwards based on the increase in the temperature gradient between IODP sites U1313 and U1385 from 706 ka to 700 ka (Fig. 8d). Other studies show relatively stable SST during MIS 17c in the eastern North Atlantic (ODP 980) contemporaneous with a clear decreasing trend westwards (U1314) (Alonso-Garcia et al., 2011; Wright and Flower, 2002) (Fig. 8c). These findings suggested that the Subpolar Front moved to the southeast but allowing the North Atlantic Current (NAC) to enter in the Norwegian Greenland Seas (NGS). This promoted deep water formation in the NGS and brought moisture and warmth towards Northern Hemisphere higher latitudes (Fig. 9). Recent results indicate a change in the circulation regime of the abyssal subtropical North Atlantic, ODP Site 1063 (Fig. 1), during MIS 17 signifying increased production of a dense deepwater mass in the NGS akin to lower North Atlantic deep water in the modern ocean (Poirier and Billups, 2014). This change predated the occurrence of the first deep glacial maximum corresponding to the establishment of strong 100-kyr cycles at ~650 ka (Poirier and Billups, 2014). These findings confirm that the “Nordic heat pump” would have replaced the “Boreal heat pump” at ~700 ka

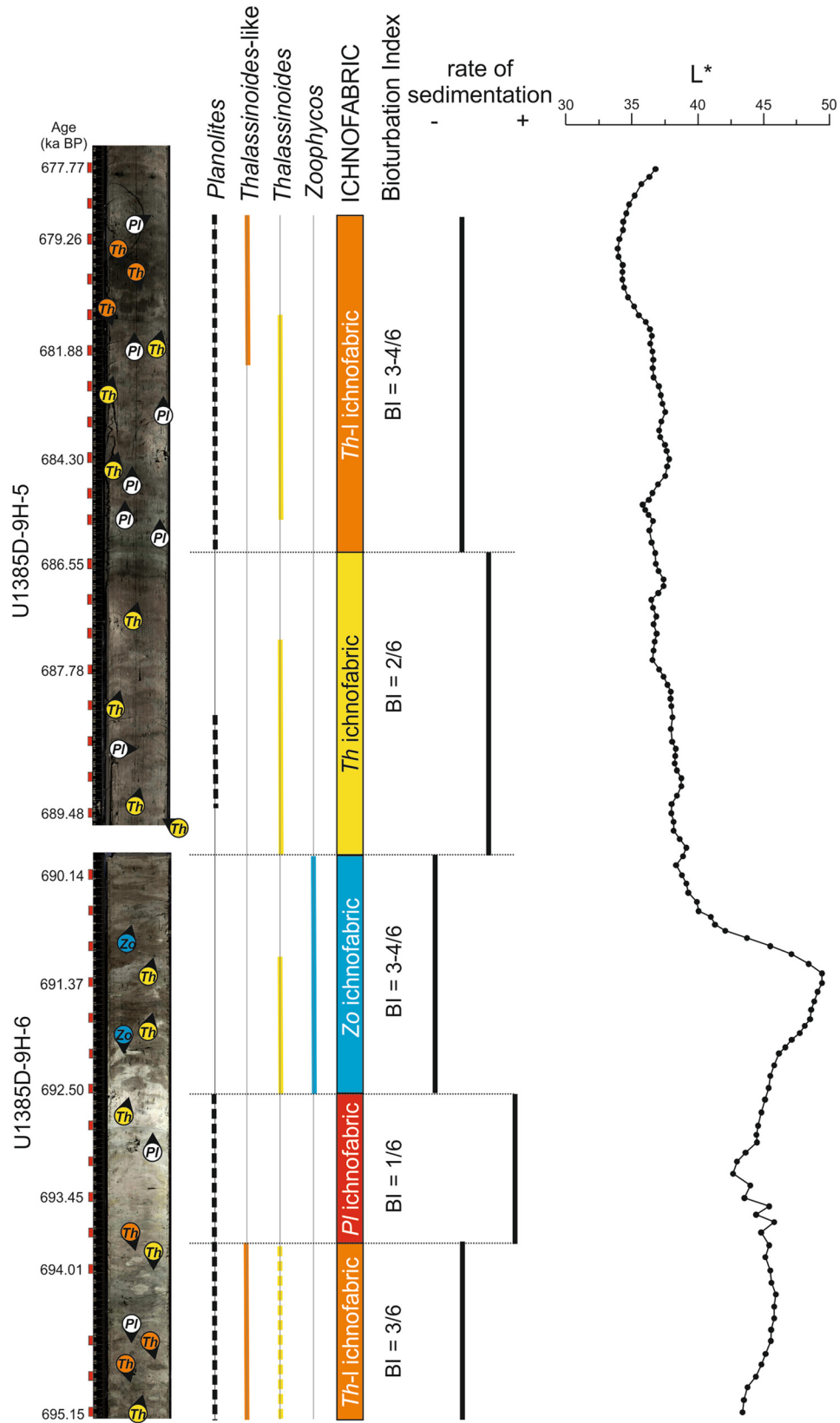


Fig. 7. Ichnological features in the interval 695.15–677.77 ka, showing the distribution of the differentiated ichnofabrics, and dominant ichnotaxa (*Pl*, *Planolites*; *Th*, *Thalassinoides*; *Th-l*, *Thalassinoides*-like; *Zo*, *Zoophycos*). BI = Bioturbation Index. On the right side, the high resolution lightness record (L^*) from the same IODP Site U1385 (Hodell et al., 2015).

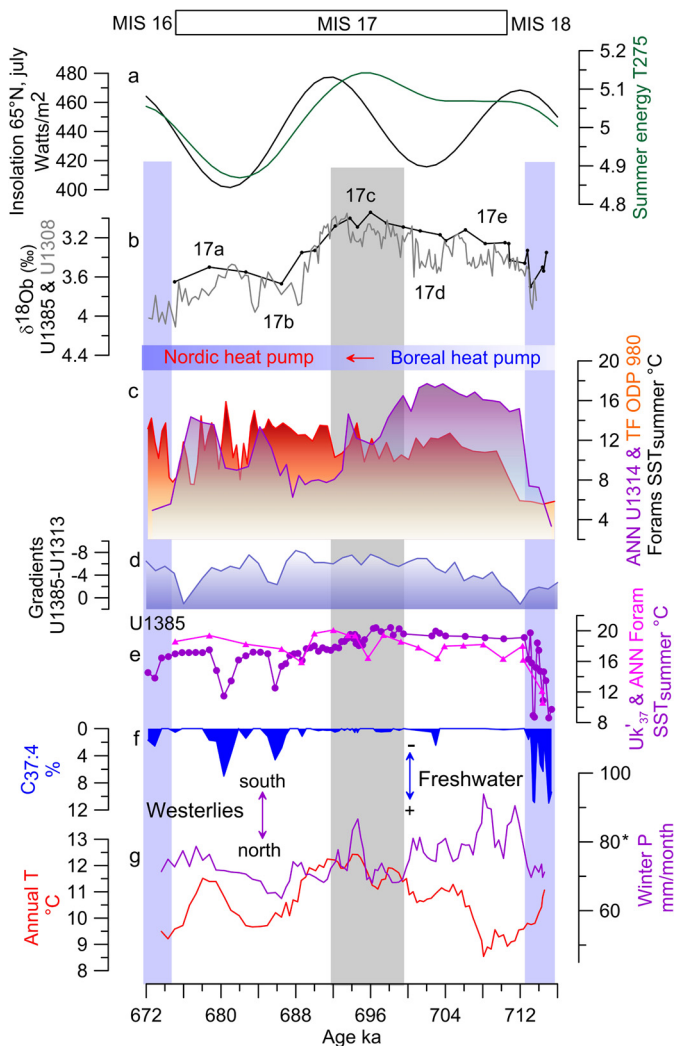


Fig. 8. Changes in atmospheric circulation in southwestern Europe inferred from pollen data, compared with orbital forcing, ice volume and oceanographic changes: (a) Summer energy (green line) and July insolation at 65°N (black line), (b) Low and high resolution $\delta^{18}\text{O}_b$ profiles from IODP sites U1385 (black line) (Hodell et al., 2015) and U1308 (grey line) (Hodell and Channell, 2016), respectively, (c) Sea Surface Temperatures (SST) in the north-central (U1314) and north-eastern (ODP 980) North Atlantic (Alonso-García et al., 2011; Wright and Flower, 2002), (d) Thermal gradient between IODP sites U1385 and U1313 (Bahr et al., 2018), (e) Foraminifera (pink triangles)- and Uk'37 (purple circles)-based SST records from the IODP site U1385 (Martín-García et al., 2015; Rodrigues et al., 2017), (f) Freshwater pulses in the Iberian margin based on the $\text{C}_{37:4}$ record of the IODP site U1385 (Rodrigues et al., 2017), (g) Pollen based mean annual temperature and winter precipitation records in southwestern Iberia (IODP site U1385; this study). Decreases in winter precipitation in southwestern Iberia during the MIS 17 interglacial indicates northward shift of the westerlies. * Present-day winter precipitation. Note that these estimations have large uncertainties (see Fig. 6). Nevertheless, the long-term changes in the average quantitative temperature and precipitation reconstructions agree with the qualitative interpretation of the pollen record. (For interpretation of the colors in the figure(s), the reader is referred to the web version of this article.)

(Imbrie et al., 1993) and additional warmth and moisture were transported to Europe as suggested for the first time by the exceptional forest expansion in southern Europe between ~696 ka and ~694 ka. This interval was marked in this region by the highest annual temperatures of MIS 17 and higher than present winter moisture (Fig. 8g), synchronous, within the age model uncertainties, with particular warm conditions in Greenland according to Barker et al.'s (2011) simulations and a peak in CH_4 concentration (Loulergue et al., 2008). Likewise, a minimum in ice volume (ice ablation related to high summer energy; Huybers, 2006) was then recorded, although moderate-sized ice sheets seem to have per-

sisted compared to other interglacials, as indicated by the $\delta^{18}\text{O}_b$ record (Lisiecki and Raymo, 2005) and the estimated changes in relative sea level (Elderfield et al., 2012) (Fig. 3b). According to Antarctic records, MIS 17 is one of the coolest interglacials of the last 800,000 yr (lukewarm interglacial) (Jouzel et al., 2007) marked by the lowest CO_2 and CH_4 concentrations (Loulergue et al., 2008; Luthi et al., 2008). Modeling studies have proposed different physical drivers to explain the displacement of winter storm tracks towards southern Europe during the early Holocene (10–8 ka) (Brayshaw et al., 2010), which resembles MIS 17c concerning residual ice caps and Mediterranean forest expansion (Oliveira et al., 2018). By analogy, the regional increase of winter rainfall during MIS 17c could be the result of three factors, low CO_2 concentration, 230–240 ppm, low boreal winter insolation that produced stronger Hadley cells and the southern position of North Atlantic storm tracks, and reduced North Atlantic latitudinal gradients of insolation and SST (Morley et al., 2014). These weak gradients are consistent with a reduced requirement for poleward energy from the subtropics to polar latitudes by the storm tracks leading to more zonal winds as shown by the Mediterranean forest expansion (Figs. 8g and 9).

During the MIS 17c/17b transition, centered at ~693 ka, the penetration of the westerlies in southern Europe weakened concomitant with still strong warm summers. These conditions indicate a still relatively northward position of the Subpolar Front associated with a major northward shift and intensification of the westerlies. At this time the eastern North Atlantic off Ireland SST slightly increased (ODP 980) reflecting strong influence of NAC water, whereas the western (ODP 647 and U1313), northern (ODP 984) and central (U1314) North Atlantic regions (Alonso-García et al., 2011; Wright and Flower, 2002) got colder, supporting a change in atmospheric conditions in the North Atlantic (Fig. 8c, 9 and Fig. S4). Concomitant with this atmospheric change associated with a drying event in southwestern Iberia, we observe locally the strongest decrease in the rate of oxygenation of the MIS 17 interval (Fig. 6 and Fig. S4) that may be related with the large scale intensification of the deep oceanic currents recorded at that time (Poirier and Billups, 2014). Increased penetration of the westerlies into high latitudes contemporaneous with decreasing summer energy probably amplified ice growth by providing additional moisture. Moreover, the slightly lower *N. pachyderma* (d) $\delta^{18}\text{O}$ values at site U1314 suggest a maximal influence of the NAC in the subpolar gyre during summer (Alonso-García et al., 2011). In this context, the warm waters of the NAC still reached Site U1314 area in summer during glacial inception and this might have introduced additional heat and moisture into the subpolar gyre promoting snow accumulation in colder North America and the surrounding areas. The west–east SST gradient, called “lagging warmth” (Wright and Flower, 2002), persisted during MIS 17b and the beginning of MIS 17a associated with intense deep water formation, sustained high $\delta^{13}\text{C}$ values (Alonso-García et al., 2011; Poirier and Billups, 2014), in the NGS additionally fueling glacial inception towards MIS 16. The decrease in summer energy (T275) certainly played an important role in snow production but the westerlies brought the moisture necessary to produce snow and subsequently strong ice accumulation. With this decrease in summer energy, higher latitudes are far too dry to provide the moisture necessary to feed the ice caps. Other processes could amplify the ice accumulation throughout MIS 16 such as the albedo feedback, which reduces ice ablation during this interval of low summer insolation. After the coalescing of the North American ice domes the hysteresis loop permitted a positive ice sheet mass balance through several precession cycles leading to the first strong and long 100-kyr ice age cycle (Abe-Ouchi et al., 2013; Hodell and Channell, 2016).

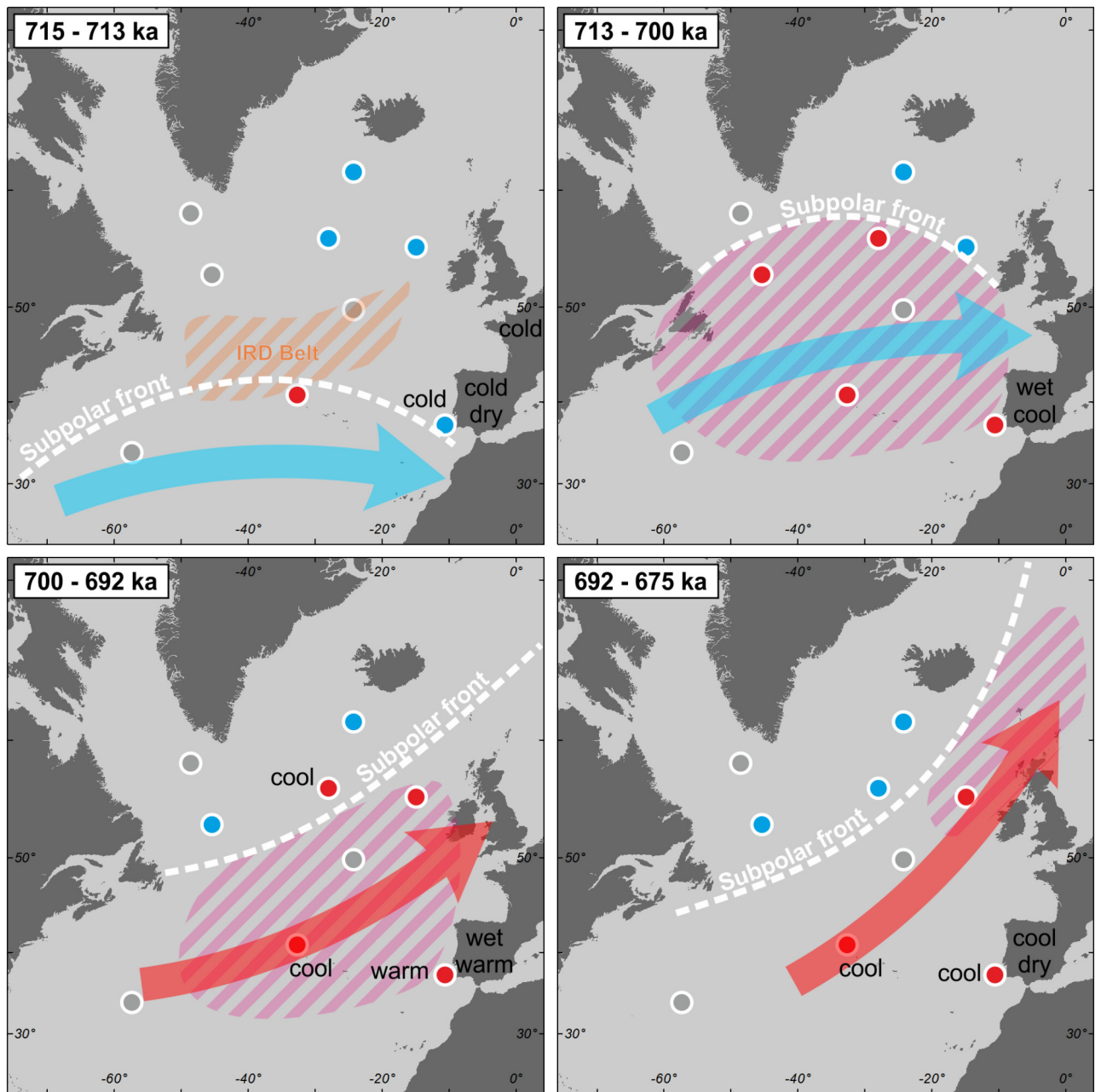


Fig. 9. Schematic overview of the atmospheric and oceanic processes evolving during MIS 17. Arrows indicate the position of the westerlies. Red circles: warm SST, blue circles: cold SST, grey circles: no SST data. Pink dashed area indicates the position of the deep water formation. (For interpretation of the colors in the figure(s), the reader is referred to the web version of this article.)

6. Conclusion

The finding that southern Europe was characterized by persistently high winter and summer moisture (twofold today's precipitation) during the cold summers of the first 15,000 yr of MIS 17 supports the hypothesis that Europe maintained well-developed Alpine glaciers between ~ 714 and 700 ka. Our data additionally supports an 18-kyr protracted deglaciation, from ~ 714 to 696 ka, longer than that modeled, ~ 6 -kyr (Parrenin and Paillard, 2012). Between ~ 700 ka and 694 ka, MIS 17d/17c transition, we infer a significant change in the atmospherically-driven vegetation record with maximum warmth and strong winter moisture in southern Europe concomitant with the progressive intensification of the deep water formation in the NGS and the decrease of the SST latitudinal gradient. The peak of winter precipitation at MIS 17c, ~ 694 ka, was followed by a pronounced two-steps northward shift

and strengthening of the westerlies that would have transported high amount of moisture to higher latitudes, thus amplifying the effect of the arrival of moisture by the warm NAC. This increase of moisture in the northern regions was contemporaneous with a decrease in summer energy and insolation at 65°N that allowed snow fall and subsequent ice sheet growth in colder Greenland, northern Europe and the Arctic during the MIS 17/16 transition, and by hysteresis lead to the final breaking point to the strong 100-kyr ice age cycles.

Acknowledgements

J.M.P.M. was funded by a Basque Government post-doctoral fellowship (POS_2015_1_0006) and MAG and TR by FCT (PTDC/MAR-PRO/3396/2014, UID/Multi/04326/2013, SFRH/BPD/96960/2013, SFRH/BPD/108600/2015). We acknowledge C. Morales-Molino and

D. Oliveira for the reading of the manuscript and V. Hanquiez for drawing Figs. 1 and 9. We are grateful to Ludovic Devaux for pollen sample preparation.

Appendix A. Supplementary material

Supplementary material related to this article can be found online at <https://doi.org/10.1016/j.epsl.2019.01.032>.

References

- Abe-Ouchi, A., Saito, F., Kawamura, K., Raymo, M.E., Okuno, J., Takahashi, K., Blatter, H., 2013. Insolation-driven 100,000-year glacial cycles and hysteresis of ice-sheet volume. *Nature* 500, 190.
- Alonso-García, M., Sierro, F.J., Kucera, M., Flores, J.A., Cacho, I., Andersen, N., 2011. Ocean circulation, ice sheet growth and interhemispheric coupling of millennial climate variability during the mid-Pleistocene (ca 800–400 ka). *Quat. Sci. Rev.* 30, 3234–3247.
- Bahr, A., Kaboth, S., Hodell, D., Zeeden, C., Fiebig, J., Friedrich, O., 2018. Oceanic heat pulses fueling moisture transport towards continental Europe across the mid-Pleistocene transition. *Quat. Sci. Rev.* 179, 48–58.
- Bai, J., Perron, P., 2003. Computation and analysis of multiple structural change models. *J. Appl. Econ.* 18, 1–22.
- Barker, S., Knorr, G., Edwards, R.L., Parrenin, F., Putnam, A.E., Skinner, L.C., Wolff, E., Ziegler, M., 2011. 800,000 years of abrupt climate variability. *Science*.
- Berger, A., Loutre, M.F., 1991. Insolation values for the climate of the last 10 million years. *Quat. Sci. Rev.* 10, 297–317.
- Berger, A., Loutre, M.F., Mélice, J.L., 2006. Equatorial insolation: from precession harmonics to eccentricity frequencies. *Clim. Past* 2, 131–136.
- Bintanja, R., van de Wal, R.S.W., 2008. North American ice-sheet dynamics and the onset of 100,000-year glacial cycles. *Nature* 454, 869.
- Blanco Castro, E., Casado González, M.A., Costa Tenorio, M., Escribano Bombín, R., García Antón, M., Génova Fuster, M., Gómez Manzaneque, F., Moreno Sáiz, J.C., Morla Juaristi, C., Regato Pajares, P., Sáiz Ollero, H., 1997. Los bosques ibéricos. *Planeta, Barcelona*. 572 p.
- Bradshaw, R.H.V., Webb III, T., 1985. Relationships between contemporary pollen and vegetation data from Wisconsin and Michigan, USA. *Ecology* 66, 721–737.
- Brayshaw, D.J., Hoskins, B., Black, E., 2010. Some physical drivers of changes in the winter storm tracks over the North Atlantic and Mediterranean during the Holocene. *Philos. Trans. R. Soc. A* 368, 5185–5223.
- Brewer, S., Guiot, J., Barboni, D., 2007. Pollen data as climate proxies. In: Elias, S.A. (Ed.), *Encyclopedia of Quaternary Science*. Elsevier, pp. 2498–2510.
- Davis, B.A.S., Zanon, M., Collins, P., Mauri, A., Bakker, J., Barboni, D., Barthelmes, A., Beaudouin, C., Bjune, A.E., Bozilova, E., Bradshaw, R.H.W., Brayshaw, B.A., Brewer, S., Brugiapaglia, E., Bunting, J., Connor, S.E., de Beaulieu, J.-L., Edwards, K., Ejarque, A., Fall, P., Florenzano, A., Fyfe, R., Galop, D., Giardini, M., Giesecke, T., Grant, M.J., Guiot, J., Jahns, S., Jankovská, V., Juggins, S., Kahrman, M., Karpíšská-Kolaczek, M., Kolaczek, P., Kühl, N., Kuneš, P., Lapteva, E.G., Leroy, S.A.G., Leydet, M., Guiot, J., López Sáez, J.A., Masí, A., Matthias, I., Mazier, F., Meltsov, V., Mercuri, A.M., Miras, Y., Mitchell, F.J.G., Morris, J.L., Naughton, F., Nielsen, A.B., Novenko, E., Odgaard, B., Ortu, E., Overballe-Petersen, M.V., Pardoe, H.S., Peglar, S.M., Pidek, I.A., Sadori, L., Seppä, H., Severova, E., Shaw, H., Świąta-Musznicka, J., Theuerkauf, M., Tonkov, S., Veski, S., van der Knaap, W.O., van Leeuwen, J.F.N., Woodbridge, J., Zimny, M., Kaplan, J.O., 2013. The European Modern Pollen Database (EMPD) project. *Veg. Hist. Archaeobot.* 22, 521–530.
- Dorador, J., Rodríguez-Tovar, F.J., 2018. High-resolution image treatment in ichnological core analysis: initial steps, advances and prospects. *Earth-Sci. Rev.* 177, 226–237.
- Dorador, J., Wetzel, A., Rodríguez-Tovar, F.J., 2016. Zoophycos in deep-sea sediments indicates high and seasonal primary productivity: ichnology as a proxy in palaeoceanography during glacial–interglacial variations. *Terra Nova* 28, 323–328.
- Ehlers, J., Gibbard, P.L., 2007. The extent and chronology of Cenozoic Global Glaciation. *Quat. Int.* 164–165, 6–20.
- Elderfield, H., Ferretti, P., Greaves, M., Crowhurst, S., McCave, I.N., Hodell, D., Piotrowski, A.M., 2012. Evolution of ocean temperature and ice volume through the mid-Pleistocene climate transition. *Science* 337, 704–709.
- Fiúza, A.F.d.G., Macedo, M.E.d., Guerreiro, M.R., 1982. Climatological space and time variation of the Portuguese coastal upwelling. *Oceanol. Acta* 5, 31–40.
- Fletcher, W.J., Sanchez Goñi, M.F., 2008. Orbital- and sub-orbital-scale climate impacts on vegetation of the western Mediterranean basin over the last 48,000 yr. *Quat. Res.* 70, 451–464.
- Gouhier, T.C., Grinsted, A., 2014. Package 'Biwavelet': R Package Version 0.20.11.
- Gouveia, C., Trigo, R.M., DaCamara, C.C., Libonati, R., Pereira, J.M.C., 2008. The North Atlantic Oscillation and European vegetation dynamics. *Int. J. Climatol.* 28, 1835–1847.
- Haeuselmann, P., Granger, D.E., Jeannin, P.-Y., Lauritzen, S.-E., 2007. Abrupt glacial valley incision at 0.8 Ma dated from cave deposits in Switzerland. *Geology* 35, 143–146.
- Hodell, D.A., Channell, J.E.T., 2016. Mode transitions in Northern Hemisphere glaciation: co-evolution of millennial and orbital variability in Quaternary climate. *Clim. Past* 12, 1805–1828.
- Hodell, D.A., Channell, J.E.T., Curtis, J.H., Romero, O.E., Röhl, U., 2008. Onset of “Hudson Strait” Heinrich events in the eastern North Atlantic at the end of the middle Pleistocene transition (~640 ka)? *Paleoceanography* 23, PA4218.
- Hodell, D., Crowhurst, S., Skinner, L., Tzedakis, P.C., Margari, V., Channell, J.E.T., Kamenov, G., Maclachlan, S., Rothwell, G., 2013. Response of Iberian Margin sediments to orbital and suborbital forcing over the past 420 ka. *Paleoceanography* 28, 185–199.
- Hodell, D.A., Lourens, L., Crowhurst, S., Konijnendijk Tjallingii, R., Jiménez-Espejo, F., Skinner, L., Tzedakis, P.C., Members, S.S.P., 2015. A reference time scale for site U1385 (Shackleton Site) on the Iberian Margin. *Glob. Planet. Change* 133, 49–64.
- Huntley, B., Birks, H.J.B., 1983. *An Atlas of Past and Present Pollenmaps for Europe: 0–13,000 B.P. Years Ago*. Cambridge University Press, Cambridge. 667 p.
- Huybers, P., 2006. Early Pleistocene glacial cycles and the integrated summer insolation forcing. *Science*.
- Imbrie, J., Berger, A., Boyle, E.A., Clemens, S.C., Duffy, A., Howard, W.R., Kukla, G.J., Kutzbach, J., Martinson, D.G., McIntyre, A., Mix, A.C., Molino, B., Morley, J.J., Peterson, L.C., Pisias, N.G., Prell, W.L., Raymo, M.E., Shackleton, N.J., Toggweiler, J.R., 1993. On the structure and origin of major glaciation cycles 2. The 100,000-year cycle. *Paleoceanography* 8, 699–735.
- Jouzel, J., Masson-Delmotte, V., Cattani, O., Dreyfus, G., Falourd, S., Hoffmann, G., Minster, B., Nouet, J., Barnola, J.M., Chappellaz, J., Fischer, H., Gallet, J.C., Johnsen, S., Leuenberger, M., Loulergue, L., Luethi, D., Oerter, H., Parrenin, F., Raisbeck, G., Raynaud, D., Schilt, A., Schwander, J., Selmo, E., Souchez, R., Spahni, R., Stauffer, B., Steffensen, J.P., Stenni, B., Stocker, T.F., Tison, J.L., Werner, M., Wolff, E.W., 2007. Orbital and millennial Antarctic climate variability over the past 800,000 years. *Science* 317, 793–796.
- Juggins, S., 2009. Package “rioja” – analysis of quaternary science data. In: *The Comprehensive R Archive Network*.
- Juggins, S., 2012. *Rioja: Analysis of Quaternary Science Data*. R Package Version (0.8-3).
- Juggins, S., Birks, H.J.B., 2011. Quantitative environmental reconstructions from biological data. In: Birks, H.J.B., Lotter, A.F., Juggins, S., Smol, J.P. (Eds.), *Tracking Environmental Change Using Lake Sediments: Data Handling and Numerical Techniques*. Springer, pp. 431–494.
- Knaust, D., 2017. *Atlas of Trace Fossils in Well Core: Appearance, Taxonomy and Interpretation*. Springer, Cham, Switzerland.
- Kollas, C., Körner, C., Randin, C.F., 2014. Spring frost and growing season length control the cold range limits of broad-leaved trees. *J. Biogeogr.* 41, 773–783.
- Lañé, A., Kageyama, M., Salas-Méila, D., Volodire, A., Rivière, G., Ramstein, G., Planton, S., Tyteca, S., Peterschmitt, J.Y., 2009. Northern hemisphere storm tracks during the last glacial maximum in the PMIP2 ocean–atmosphere coupled models: energetic study, seasonal cycle, precipitation. *Clim. Dyn.* 32, 593–614.
- Lisiecki, L., Raymo, M.E., 2005. A Pliocene–Pleistocene stack of 57 globally distributed benthic $\delta^{18}\text{O}$ records. *Paleoceanography* 20, PA1003.
- Liu, Y., San Liang, X., Weisberg, R.H., 2007. Rectification of the bias in the wavelet power spectrum. *J. Atmos. Ocean. Technol.* 24, 2093–2102.
- Loulergue, L., Schilt, A., Spahni, R., Masson-Delmotte, V., Blunier, T., Lemieux, B., Barnola, J.-M., Raynaud, D., Stocker, T.F., Chappellaz, J., 2008. Orbital and millennial-scale features of atmospheric CH_4 over the past 800,000 years. *Nature* 453, 383–386.
- Luthi, D., Le Floch, M., Bereiter, B., Blunier, T., Barnola, J.-M., Siegenthaler, U., Raynaud, D., Jouzel, J., Fischer, H., Kawamura, K., Stocker, T.F., 2008. High-resolution carbon dioxide concentration record 650,000–800,000 years before present. *Nature* 453, 379–382.
- MacEachern, J.A., Bann, K.L., Gingras, M.K., Zonneveld, J.P., Dashtgard, S.L., Pemberton, G., 2012. The ichnofacies paradigm. In: Knaust, D., Bromley, R.G. (Eds.), *Trace Fossils as Indicators of Sedimentary Environments*. In: *Developments in Sedimentology*, vol. 64. Elsevier, pp. 103–138.
- Marchal, O., Waelbroeck, C., Verdère, A.C.d., 2016. On the movements of the North Atlantic Subpolar Front in the preinstrumental past. *J. Climate* 29, 1545–1571.
- Martin-García, G.M., Alonso-García, M., Sierro, F.J., Hodell, D.A., Flores, J.A., 2015. Severe cooling episodes at the onset of deglaciations on the southwestern Iberian margin from MIS 21 to 13 (IODP site U1385). *Glob. Planet. Change* 135, 159–169.
- Mauri, A., Davis, B.A.S., Collins, P.M., Kaplan, J.O., 2015. The climate of Europe during the Holocene: a gridded pollen-based reconstruction and its multi-proxy evaluation. *Quat. Sci. Rev.* 112, 109–127.
- Meijer, P.T., Tuenter, E., 2007. The effect of precession-induced changes in the Mediterranean freshwater budget on circulation at shallow and intermediate depth. *J. Mar. Syst.* 68, 349–365.
- Miranda, P.M.A., Coelho, F.E.S., Tomé, A.R., Valente, M.A., Carvalho, A., Pires, C., Pires, H.O., Pires, V.C., Ramalho, C., 2002. 20th century Portuguese climate and climate scenarios. In: Santos, F.D., Forbes, K., Moita, R. (Eds.), *Climate Change in Portugal: Scenarios, Impacts and Adaptation Measures (SIAM Project)*. Gradiva, pp. 23–83.
- Morley, A., Rosenthal, Y., deMenocal, P., 2014. Ocean–atmosphere climate shift during the mid-to-late Holocene transition. *Earth Planet. Sci. Lett.* 388, 18–26.

- Mudelsee, M., Statterger, K., 1997. Exploring the structure of the mid-Pleistocene revolution with advanced methods of time-series analysis. *Geol. Rundsch.* 86, 499–511.
- Naafs, B.D.A., Hefter, J., Ferretti, P., Stein, R., Haug, G.H., 2011. Sea surface temperatures did not control the first occurrence of Hudson Strait Heinrich Events during MIS 16. *Paleoceanography* 26, PA4201.
- Naafs, B.D.A., Hefter, J., Stein, R., 2013. Millennial-scale ice rafting events and Hudson Strait Heinrich(-like) Events during the late Pliocene and Pleistocene: a review. *Quat. Sci. Rev.* 80, 1–28.
- Nieto-Lugilde, D., Maguire, K.C., Blois, J.L., Williams, J.W., Fitzpatrick, M.C., 2015. Close agreement between pollen-based and forest inventory-based models of vegetation turnover. *Glob. Ecol. Biogeogr.*
- Ogawa, F., Nakamura, H., Nishii, K., Miyasaka, T., Kuwano-Yoshida, A., 2012. Dependence of the climatological axial latitudes of the tropospheric westerlies and storm tracks on the latitude of an extratropical oceanic front. *Geophys. Res. Lett.* 39.
- Oliveira, D., Desprat, S., Yin, Q., Naughton, F., Trigo, R., Rodrigues, T., Abrantes, F., Sánchez Goñi, M.F., 2018. Unraveling the forcings controlling the vegetation and climate of the best orbital analogues for the present interglacial in SW Europe. *Clim. Dyn.* 51, 667–686.
- Parrenin, F., Paillard, D., 2012. Terminations VI and VIII (~530 and ~720 kyr BP) tell us the importance of obliquity and precession in the triggering of deglaciations. *Clim. Past* 8, 2031–2037.
- Poirier, R.K., Billups, K., 2014. The intensification of northern component deepwater formation during the mid-Pleistocene climate transition. *Paleoceanography* 29, 1046–1061.
- Polunin, O., Walters, M., 1985. *A Guide to the Vegetation of Britain and Europe*. Oxford University Press, New York. 238 p.
- Prentice, I.C., Guiot, J., Harrison, S.P., 1992. Mediterranean vegetation, lake levels and palaeoclimate at the Last Glacial Maximum. *Nature* 360, 658.
- R Development Core, T., 2011. *R: A Language and Environment for Statistical Computing*. R Foundation for Statistical Computing, Vienna, Austria.
- Railsback, L.B., Gibbard, P.L., Head, M.J., Voarintsoa, N.R.G., Toucanne, S., 2015. An optimized scheme of lettered marine isotope substages for the last 1.0 million years, and the climatostratigraphic nature of isotope stages and substages. *Quat. Sci. Rev.* 111, 94–106.
- Ramos, A., Trigo, R.M., Santo, F.E., 2011. Evolution of extreme temperatures in Portugal: reporting on recent changes and future scenarios. *Clim. Res.* 48, 177–192.
- Ríos, A.F., Pérez, F.F., Fraga, F., 1992. Water masses in the upper and middle North Atlantic Ocean east of the Azores. *Deep-Sea Res., Part A, Oceanogr. Res. Pap.* 39, 645–658.
- Rodrigues, T., Alonso-García, M., Hodell, D.A., Rufino, M., Naughton, F., Grimalt, J.O., Voelker, A.H.L., Abrantes, F., 2017. A 1-Ma record of sea surface temperature and extreme cooling events in the North Atlantic: a perspective from the Iberian Margin. *Quat. Sci. Rev.* 172, 118–130.
- Rodríguez-Tovar, F.J., Dorador, J., 2014. Ichnological analysis of Pleistocene sediments from the IODP Site U1385 “Shackleton Site” on the Iberian margin: approaching paleoenvironmental conditions. *Palaeogeogr. Palaeoclimatol. Palaeoecol.* 409, 24–32.
- Rodríguez-Tovar, F.J., Uchman, A., 2008. Bioturbational disturbance of the Cretaceous–Palaeogene (K–Pg) boundary layer: implications for the interpretation of the K–Pg boundary impact event. *Geobios* 41, 661–667.
- Salvo Tierra, E., 1990. *Guía de helechos de la Península Ibérica y Baleares*. Madrid.
- Sánchez Goñi, M.F., Desprat, S., Fletcher, W.J., Morales del Molino, C., Naughton, F., Oliveira, D., Urrego, D.H., Zorzi, C., 2018. Pollen from the deep-sea: a breakthrough in the mystery of the Ice Ages. *Front. Plant Sci.* 9.
- Sánchez Goñi, M.F., Hannon, G., 1999. High altitude vegetational patterns on the Iberian Mountain chain (north-central Spain) during the Holocene. *Holocene* 9, 39–57.
- Sánchez Goñi, M.F., Rodrigues, T., Hodell, D.A., Polanco-Martínez, J.M., Alonso-García, M., Hernández-Almeida, I., Desprat, S., Ferretti, P., 2016. Tropically-driven climate shifts in southwestern Europe during MIS 19, a low eccentricity interglacial. *Earth Planet. Sci. Lett.* 448, 81–93.
- Schulz, M., Mudelsee, M., 2002. REDFIT: estimating red-noise spectra directly from unevenly spaced paleoclimatic time series. *Comput. Geosci.* 28, 421–426.
- Stow, D.A.V., Hernández-Molina, F.J., Alvarez Zarikian, C.A., Expedition 339 Scientists, 2013. *Proceedings IODP, vol. 339. Integrated Ocean Drilling Program Management International, Inc., Tokyo.*
- Taylor, A., Goldring, R., 1993. Description and analysis of bioturbation and ichnofabric. *Q. J. Geol. Soc. Lond.* 150, 141–148.
- Toti, F., 2015. Interglacial vegetation patterns at the early–middle Pleistocene transition: a point of view from the Montalbano Jonico section (Southern Italy). *Alpine Mediterr. Q.* 28, 131–143.
- Turon, J.-L., Lézine, A.-M., Denèfle, M., 2003. Land-sea correlations for the last glaciation inferred from a pollen and dinocyst record from the Portuguese margin. *Quat. Res.* 59, 88–96.
- Valla, P.G., Shuster, D.L., van der Beek, P.A., 2011. Significant increase in relief of the European Alps during mid-Pleistocene glaciations. *Nat. Geosci.* 4, 688.
- Williams, J.W., Jackson, S.T., 2003. Palynological and AVHRR observations of modern vegetational gradients in eastern North America. *Holocene* 13, 485–497.
- Wright, A.K., Flower, B.P., 2002. Surface and deep ocean circulation in the subpolar North Atlantic during the mid-Pleistocene revolution. *Paleoceanography* 17, 20–1–20–16.
- Zeileis, A., Leisch, F., Hornik, K., Kleiber, C., 2002. *Strucchange: an R package for testing for structural change in linear regression models*. *J. Stat. Softw.* 7, 1–38.